EarthArXiv Cover Sheet

Title:

Detecting and Explaining Persistent Road Underdevelopment in Greater Accra Region Using Multi-Temporal Geospatial Data and Machine Learning

Authors

Desmond Kemeh[1]

Yuri Ribakov[1]

Klein Israel[2]

Achituv Cohen[1]

Affiliations

[1] Department of Civil Engineering, Ariel University, Ariel, Israel.

[2] Department of Economics and Business Administration, Ariel University, Ariel, Israel.

Corresponding Author

Desmond Kemeh

Email: dkemeh1@gmail.com

Preprint Status Statement

This paper is a non-peer-reviewed preprint submitted to EarthArXiv.

This manuscript has been submitted to GIScience & Remote Sensing for peer review.

Detecting and Explaining Persistent Road Underdevelopment in Greater Accra Region Using Multi-Temporal Geospatial Data and Machine Learning

Desmond Kemeh1,5*, Yuri Ribakov1,2,5, Klein Israel1,3,6 and Achituv Cohen1,4,5

1 Ariel University

2 ribakov@ariel.ac.il

3 iklein@ariel.ac.il

4 achituv@ariel.ac.il

5 Department of Civil Engineering

6 The Department of Economics and Business Administration

* Correspondence: dkemeh1@gmail.com

Abstract

Uneven transport infrastructure development remains a persistent challenge in rapidly urbanising cities, where disparities in road conditions shape mobility, accessibility, and socio-economic opportunities. In Greater Accra, Ghana, rapid urban expansion has produced a road network characterised by strong spatial inequalities, with many neighbourhood roads remaining unpaved despite surrounding development. This study identifies and quantifies persistent road underdevelopment using a reproducible geospatial and machine learning framework integrating OpenStreetMap data with multi-temporal satellite imagery (Landsat-8, Sentinel-1, and Sentinel-2). Road segments were standardised and classified using Random Forest, XGBoost, and LightGBM with spatial cross-validation. Results show that Sentinel-2 combined with LightGBM performed best, achieving a balanced accuracy of about 0.80 and an MCC of about 0.58. Change detection revealed that approximately 11,030.9 km of roads remained persistently unpaved between 2018 and 2024, representing 27.20% of the total road network. Within the urban core, 2,092 km of persistently unpaved roads were identified, compared with 1,593 km of roads upgraded from unpaved to paved. Persistent unpaved roads were spatially clustered, with 14 blind spots identified across 17 districts, covering about 566.9 km². Blind spot areas exhibited significantly higher built-up intensity than non-blind areas, supported by Mann–Whitney ($p < 0.001$), Welch

t-test ($p < 0.05$), and a large effect size (Cliff's $\delta = 0.6211$). Moran's I (0.0803, $p = 0.001$) confirmed significant spatial clustering. Overall, persistent road underdevelopment is spatially structured and associated with uneven urban development.

Keywords: Road Surface Classification, Persistent Infrastructure Underdevelopment, Geospatial Machine Learning, Spatial Clustering.

1. Introduction

Uneven transport infrastructure development is a persistent challenge in rapidly urbanising cities, where access to roads strongly shapes mobility, economic opportunity, and everyday urban life (Adugbila, Martinez and Pfeffer, 2023a). In Accra, Ghana, decades of expansion have produced a road network characterised by sharp spatial contrasts: while primary corridors have benefited from repeated investment, many neighbourhood roads remain unpaved, deteriorated, or intermittently maintained (Amedzro *et al.*, 2024). These disparities constrain everyday mobility and contribute to long-term socio-spatial inequality, particularly in contexts where road development privileges some communities over others (Adugbila, Martinez and Pfeffer, 2023a; Fobosi and Malima, 2025).

Urban transport infrastructure in rapidly growing African cities is widely described as developing more slowly and more unevenly than the urbanisation processes it is meant to support. According to World Bank (2022) transport systems in many Africa cities have failed to keep pace with urban growth, producing deficits in reliability and safe transport services to meet the travel needs of the people. In a related regional review, El-bouayady and Radoine (2023) highlights a discrepancy between current urbanization trends and urban infrastructure development in Africa, showing that this disparity manifests across sectors such as transport in infrastructure overload, lack of investment, and inadequate service provision. Khalil and Rubin (2020) similarly argues that infrastructure inequality is both an outcome and a producer of urban inequality, because localized deficits in service provision become embedded in the spatial structure of cities and reinforce longer-term disadvantage. At the same time, broad urban indicators can conceal substantial internal variation: analyses of African city form show strong centre–periphery gradients in population distribution, land cover, and paved-road provision, with peripheral areas often exhibiting weaker connectivity and accessibility (Antos, Lall and Lozano-Gracia, 2016). Together, these studies suggest that uneven road development in Accra should be understood not merely as a transport-sector issue, but as part of a wider urban process through which infrastructure provision and socio-spatial inequality co-evolve.

Such uneven development often reflects policy blind spots, areas repeatedly overlooked in transport infrastructure planning and investment cycles (Amedzro *et al.*, 2024). Over time, these blind

spots become entrenched, allowing underdeveloped roads to persist even as surrounding areas experience growth (Adugbila, Martinez and Pfeffer, 2023a; Amedzro *et al.*, 2024). While existing studies document fragmented road development and uneven accessibility in Accra, evidence on where blind spots occur, how they evolve, and why they persist remains largely descriptive (Adugbila, Martinez and Pfeffer, 2023a; Amedzro *et al.*, 2024). This study therefore focuses specifically on persistent patterns of road underdevelopment, identified through multi-temporal analysis of road surface conditions.

In this study, the term policy blind spot refers to a spatially persistent zone of under-provision, under-maintenance, or planning neglect that remains weakly served even as nearby urbanisation intensifies. This interpretation is consistent with scholarship showing that infrastructure deficits are not merely technical shortfalls, but are shaped by broader urban processes, including spatial inequality, governance arrangements, and relations of power (Gore and Gopakumar, 2015; Khalil and Rubin, 2020; Keith and De Souza Santos, 2021). Rather than treating blind spots as directly observed policy declarations, this study interprets persistent clusters of underdeveloped neighbourhood roads as spatial patterns consistent with planning omission, uneven investment, or prolonged maintenance neglect. In this context, blind spots are understood as non-random patterns of persistent road underdevelopment within the urban system.

Most prior research has examined Accra's road network using geometric or network-level approaches that focus on connectivity and structural performance (Korah, Matthews and Tomerini, 2019). However, such approaches often equate proximity to infrastructure with access. Yet proximity to roads does not necessarily translate into meaningful access for all residents (Addae and Oppelt, 2019; Akubia and Bruns, 2019). This highlights the relevance of transport-related social exclusion, which arises when access to opportunities is constrained by interacting spatial, social, economic, and infrastructural barriers such as affordability, safety, and suitability of transport options (Tossoukpe *et al.*, 2025). In Accra, persistent neighbourhood road underdevelopment therefore represents not only a technical deficit but also a mechanism through which mobility disadvantage is reproduced, particularly for residents without private vehicles (Addae and Oppelt, 2019; Osman *et al.*, 2022).

A growing body of transport scholarship argues that infrastructure should not be evaluated only by its physical presence or network geometry, but by the extent to which it enables different groups to reach opportunities in practice. Wee, Wee and Geurs (2011) shows that conventional transport

appraisal often underrepresents equity and social exclusion, because it tends to focus on aggregate efficiency rather than on how access is distributed across groups and places. Brussel *et al.* (2019) make a closely related point by arguing that Sustainable Development Goals 11.2 is supply oriented, measuring access to transportation infrastructure rather than accessibility to activity locations, and that such infrastructure-based indicators oversimplify the transport system and can hide existing spatial and socio-economic inequalities. Following the social exclusion literature, transport disadvantage emerges through interactions between mobility constraints and wider forms of social disadvantage, rather than through transport variables alone (Schwanen *et al.*, 2015). Hidayati, Tan and Yamu (2021) conceptualize mobility inequality as arising from both extrinsic spatial conditions and intrinsic, socially differentiated capacities that shape how people can turn transport access into actual mobility opportunities.

Other empirical evidence also indicates that accessibility plays a critical role in shaping participation in daily activities. For instance, it was demonstrated that low accessibility can severely restrict individuals' life chances by limiting their ability to participate in work, education, and other activities, thereby increasing the risk of social exclusion (Luz *et al.*, 2022). Morover, formal and informal urban areas in sub-Saharan African cities experience markedly different levels of walking accessibility to healthcare facilities, highlighting significant intra-urban disparities in infrastructure-based service access (Friesen, Georganos and Haas, 2025). Taken together, this literature suggests that transport infrastructure should be understood not merely as a physical network but as a system that shapes people's ability to reach opportunities. From this perspective, the persistence of unpaved neighbourhood roads in Accra may represent more than a geometric deficiency in the road network; it may also constitute a source of mobility disadvantage and transport-related social exclusion for residents whose daily activities depend on these local roads.

Recent studies show that open geospatial data and machine learning can generate spatially extensive infrastructure evidence in data-constrained settings. Raji *et al.* (2024) show that multispectral satellite imagery combined with OpenStreetMap can classify paved and unpaved roads across Sub-Saharan Africa and support multitemporal assessment of road-surface conditions. It was shown that openly available imagery and crowdsourced road data can be used to build high-quality national road-surface datasets (Zhou, Liu and Huang, 2024). Multisource open geospatial variables combined with

deep learning can identify paved and unpaved road surfaces at national scale, with road class and settlement-related variables emerging as influential predictors (Zhou, Liu and Liu, 2025). Machine learning can also move beyond simple surface detection toward the prediction of unpaved road condition, which is particularly relevant where maintenance information is (Workman *et al.*, 2023). It was demonstrated that high-resolution satellite imagery can be used to predict road quality with strong transferability across contexts, including a Nigerian case where the model distinguished paved from unpaved roads with high accuracy (Brewer *et al.*, 2021). At the same time, the value of data-driven urban analysis in African cities depends on careful decisions about data quality, validation, local relevance, and institutional capacity (Agyemang *et al.*, 2024). These studies justify the present study's use of open road data, satellite imagery, and interpretable machine learning, while also supporting the need for a reproducible and spatially robust workflow tailored to Greater Accra's specific urban conditions.Accra's uneven road development also needs to be understood against the backdrop of a metropolitan region that has expanded in a highly differentiated way across districts and peri-urban corridors. Previous studies have shown that infrastructure and service provision in Accra is spatially unequal, with significant disparities in accessibility across urban and peri-urban areas (Kyere-Gyeabour, Sivakumar and Agyei-Mensah, 2024). Accra's urban development has evolved in a fragmented and discontinuous manner over time, with distinct spatial dynamics across concentric zones of the metropolitan region, yet the overall spatial structure remains predominantly monocentric rather than polycentric (Korah, Matthews and Tomerini, 2019). Similarly, urban expansion in the Greater Accra Metropolitan Area is spatially uneven and directionally differentiated, with peri-urban frontier growth particularly concentrated in eastern and western peripheral districts of the metropolitan region (Akubia and Bruns, 2019). It was further shown that built-up land in the Greater Accra Metropolitan area has expanded dramatically over the past decades and is projected to continue expanding into adjoining districts, highlighting the spatially uneven nature of urban growth within the metropolitan region (Addae and Oppelt, 2019). More recent work also confirms that the region's urbanisation remains highly dynamic and spatially selective: Substantial outward expansion of built-up land in the Greater Accra Metropolitan area was documented (Tossoukpe *et al.*, 2025), while land consumption patterns are strongly influenced by anthropogenic drivers such as population dynamics and socio-economic factors (Osman *et al.*, 2022). For that reason, this study does not treat district boundaries as mere reporting

units; rather, districts provide an administratively meaningful scale for showing how persistent road underdevelopment intersects with the metropolitan geography of expansion, consolidation, and uneven investment

The present study aims to identify, quantify, and explain the persistence of road underdevelopment in Greater Accra, Ghana using a reproducible geospatial and machine learning framework. Specifically, the approach is designed to answer three key questions: where persistent underdevelopment occurs, how it is spatially structured, and what spatial factors are associated with its persistence. To achieve this, the study applies a reproducible geospatial workflow combining satellite imagery, OSM data, and machine learning to classify road surface conditions across time. Spatial analytical techniques, including kernel density estimation and spatial autocorrelation analysis, are then used to identify clusters of persistent underdevelopments and examine their relationship with urban development patterns.

2. Materials and Methods

Figure 1 provides an overview of the methodological framework used in this study. The workflow integrates open road network data, multi-sensor satellite imagery, spatial machine learning, change detection, and spatial analysis. The process begins with extracting road surface labels from OSM and segmenting the road network into uniform 100 m units. Satellite-derived features are then extracted from Landsat-8, Sentinel-2, and Sentinel-1 imagery for each road segment. These features are used to train machine learning models to classify road surfaces as paved or unpaved for 2018 and 2024. The resulting predictions are compared across years to detect road surface changes, after which spatial analysis techniques are applied to identify clusters of persistently unpaved roads and analyse their spatial distribution across Greater Accra Region of Ghana.

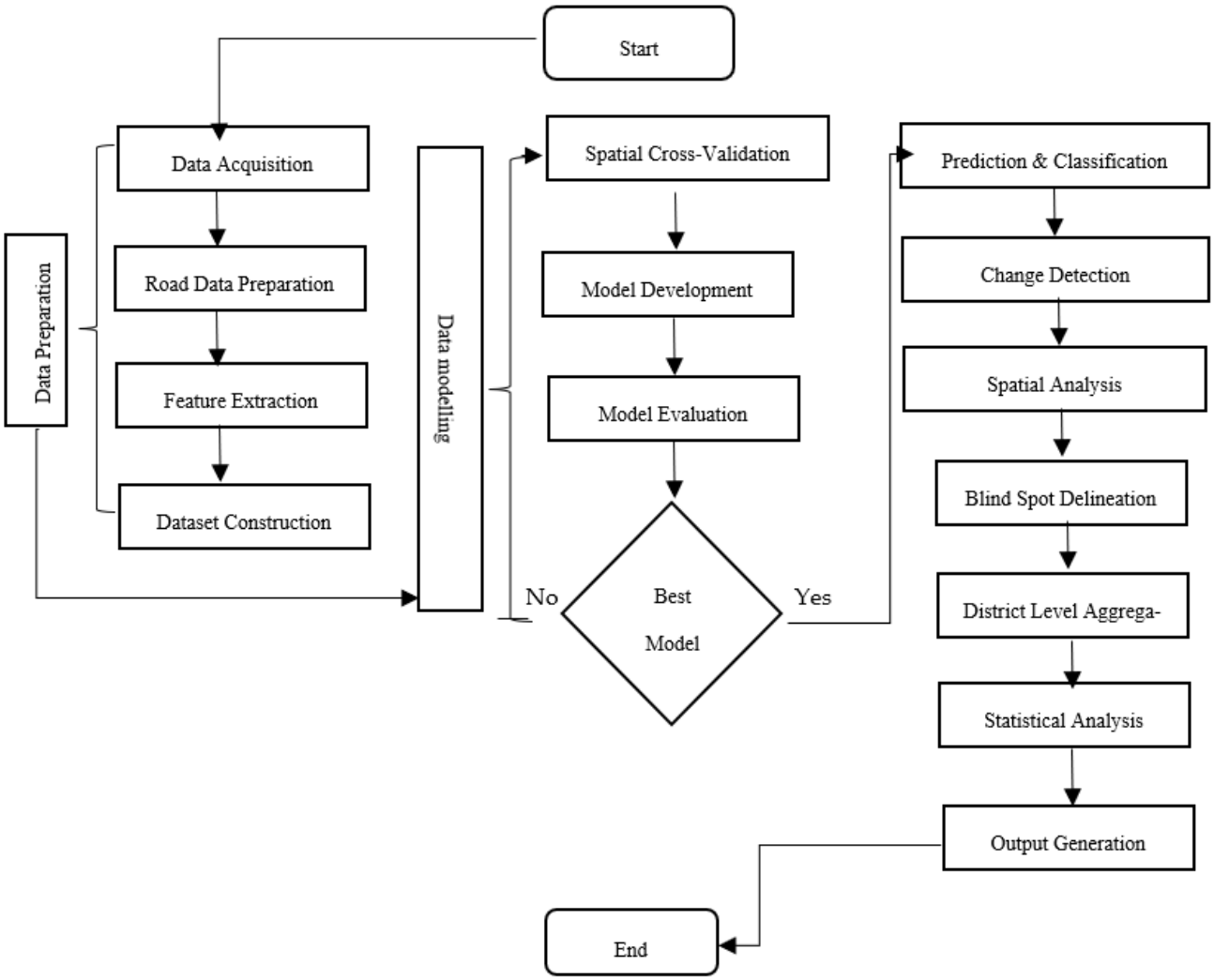

Figure 1: Methodological workflow for detecting persistent road underdevelopment in Greater Accra. The framework integrates open road network data, multi-sensor satellite imagery, spatial machine learning, change detection, and spatial-statistical analysis to identify and characterize blind spot areas.

2.1 Study Area

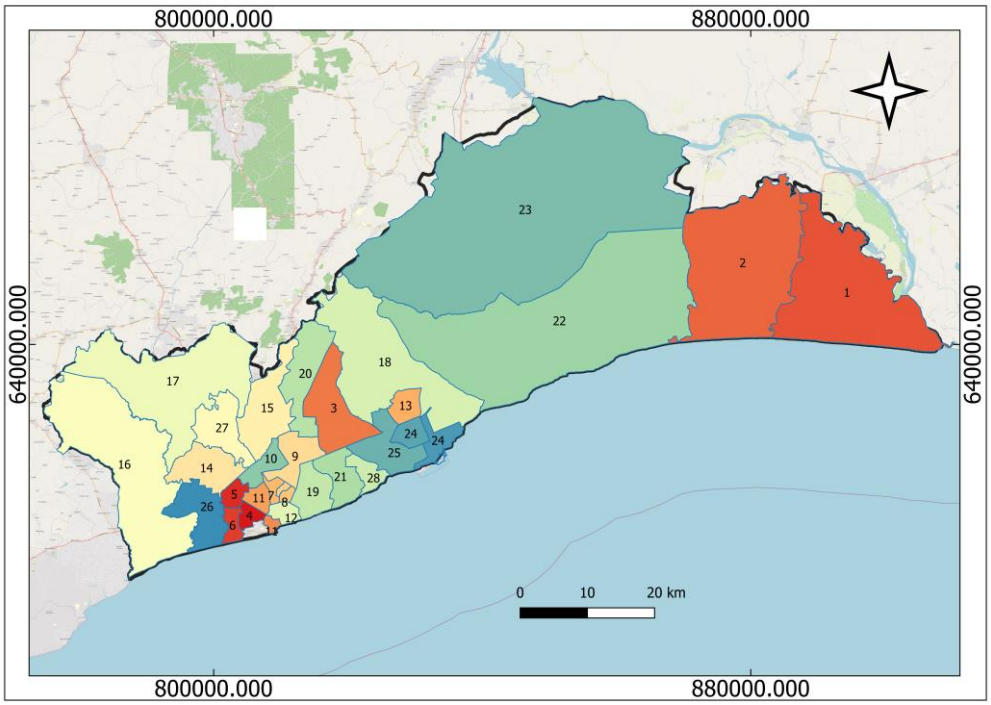

LEGEND

1 Ada East
2 Ada West
3 Adenta Municipal
4 Ablekuma Central Municipal
5 Ablekuma North Municipal
6 Ablekuma West Municipal
7 Ayawaso Central Municipal
8 Ayawaso East Municipal
9 Ayawaso West
10 Okaikwei North Municipal
11 Accra Metropolitan
12 Korle-Klottey Municipal
13 Ashaiman Municipal
14 Ga Central Municipal
15 Ga East Municipal
16 Ga South Municipal
17 Ga West Municipal
18 Kpone Katamanso Municipal
19 La Dade-Kotopon
20 La Nkwantanang-Madina
21 Ledzokuku Municipal
22 Ningo-Prampram
23 Shai Osudoku
24 Tema Metropolitan
25 Tema West Municipal
26 Weija-Gbawe Municipal
27 Ga North Municipal
28 Krowor Municipal
29 Ayawaso North Municipal

(a)

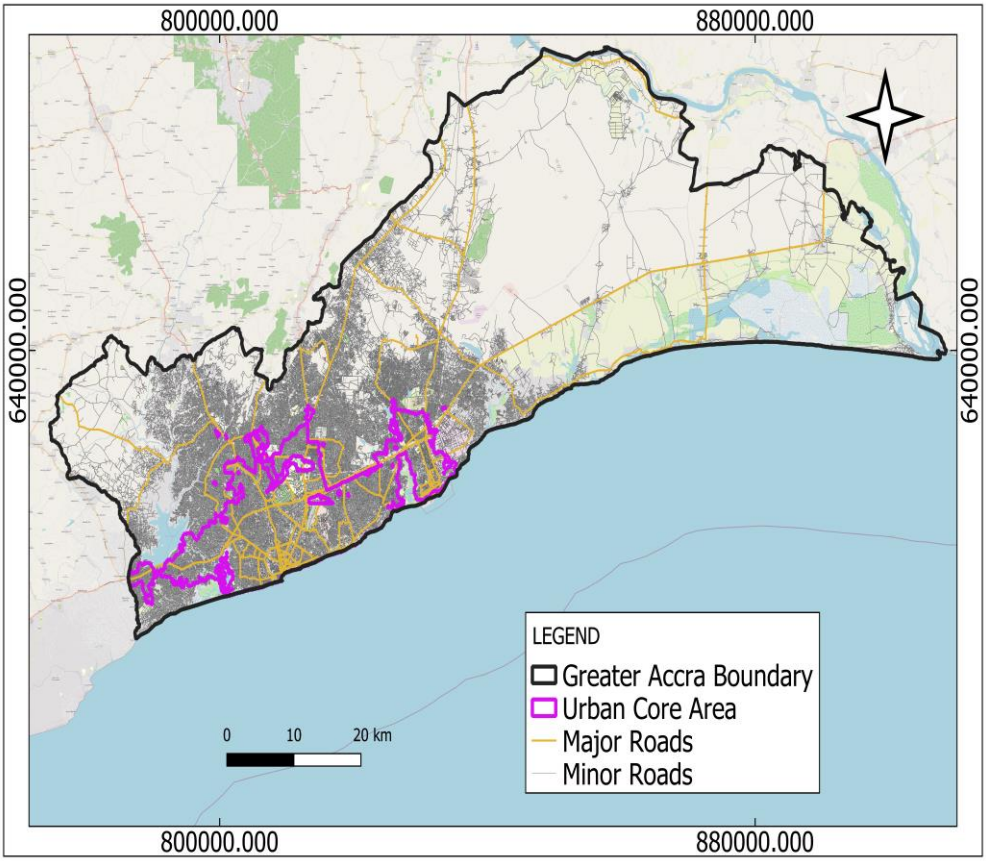

(b)

(c)

(d)

Figure 2. Map of the Study Area.

The study focuses on the Greater Accra Region of Ghana, located along the Gulf of Guinea in the southern part of the country. The region is part of West Africa, where urbanisation is among the fastest growing globally, with Greater Accra experiencing rapid population growth and urban expansion (Tossoukpe *et al.*, 2025). This rapid urban growth has produced strong spatial contrasts between the historic urban core and newly developing peripheral districts, shaping patterns of accessibility and

infrastructure provision across the metropolitan area (Acheampong, Asabere and Asuah, 2022). The Greater Accra Region is divided into 29 Metropolitan, Municipal and District Assemblies (MMDAs), as shown in Figure 2(a), which serve as the primary administrative units for planning and governance. The region comprises highly urbanised districts concentrated around central Accra, alongside rapidly expanding peri-urban and peripheral districts where development continues to extend outward.

Within this metropolitan system, the historic urban core (Accra Central) is shown in Figure 2(b) as a distinct zone characterised by relatively higher levels of infrastructure provision and accessibility. In contrast, many peripheral districts experience ongoing urban expansion with comparatively uneven infrastructure development. This contrast provides a suitable context for examining spatial patterns of persistent road underdevelopment. Figure 2(b) further distinguishes major and minor roads using OSM highway classifications, where motorway, trunk, primary and secondary roads represent major transport corridors, and tertiary, residential and unclassified roads represent neighbourhood streets. This classification provides a spatial reference for analysing how persistent unpaved road segments are distributed across different parts of the metropolitan road network. Figures 2(c) and 2(d) provide photographic examples of the road surface conditions examined in this study. Figure 2(c) shows an unpaved road, illustrating the type of neighbourhood road environment associated with limited surface improvement and potentially lower accessibility, particularly during adverse weather conditions. Figure 2(d) shows a paved road, representing a more formally improved road surface.

2.2 Data Sources

The study used OSM road network snapshots together with Landsat-8, Sentinel-2, Sentinel-1, and the Global Human Settlement Layer (GHSL) because earlier research has shown that urban mapping in data-scarce settings can be strengthened by combining Earth observation data with volunteered geographic information and other geospatial layers.

In Sub-Saharan Africa, Forget *et al.* (2021) explicitly proposed that urban mapping in Sub-Saharan Africa is constrained by the limited availability of reference datasets for training and validation. To address this challenge, they propose a mapping approach that integrates multi-sensor satellite imagery with volunteered geographic information from OSM, while Forget, Linard and Gilbert (2018)

showed that OSM can be used to automatically collect training samples for supervised learning and reported that OSM-based classifications can perform similarly to classifications built from manually digitized samples when OSM training information is sufficiently available and properly pre-processed. In the present study, OSM was therefore used as the road framework and, where available, its road attributes were used to derive weak labels for model training. The years 2018 and 2024 were selected for this study because imagery from Landsat-8, Sentinel-2, and Sentinel-1 were available across all three sensors for those years for the study area, allowing direct cross-sensor comparison under a harmonized analytical design.

For the contextual interpretation of persistent road underdevelopment, GHSL built-up data were utilized to derive spatially explicit measures of settlement intensity across the study area. The GHSL dataset provides grid-based (raster) representations of built-up presence derived from satellite imagery and has been widely applied in the mapping and analysis of urbanization patterns and settlement structure (Melchiorri *et al.*, 2019). In this study, the GHSL built-up raster was integrated within a GIS framework to derive spatial attributes using zonal statistics, a widely used method for aggregating raster information within defined spatial units. This approach enabled the extraction of mean built-up intensity values for both blind spot and non-blind spot areas, facilitating a comparative assessment of settlement patterns in relation to road network underdevelopment.

Within the remote sensing component of the study, Landsat-8, Sentinel-2, and Sentinel-1 were analysed separately to assess how effectively each sensor captures urban surface characteristics associated with neighbourhood road conditions. Landsat-8 was retained because the long-running Landsat programme provides a globally consistent archive for monitoring urban expansion and land-cover change. Landsat-based approaches have been shown to map long-term urban growth across Sub-Saharan African cities, making Landsat-8 suitable for capturing broad patterns of urban surfaces and land cover around road infrastructure (Forget *et al.*, 2021).

Sentinel-2 was included because its multispectral imagery, with spatial resolutions of up to 10 m, supports more detailed mapping of land cover and urban environments. The sensor is widely used for land-cover monitoring because of its high spatial resolution, short revisit time, multiple spectral bands, and free data access (Phiri *et al.*, 2020). Sentinel-2 has also been shown to improve the detection of

built-up areas by offering finer spatial and spectral detail (Pesaresi *et al.*, 2016). These features make it useful for examining neighbourhood-scale variation in urban surface conditions along road corridors.

Sentinel-1 differs from the two optical sensors because it provides information from microwave backscatter rather than reflected sunlight. Radar observations can be acquired independently of daylight and are largely unaffected by cloud cover, which makes them particularly useful where atmospheric conditions constrain optical imagery (Mahmoud *et al.*, 2022). Radar signals also interact strongly with built structures, helping to identify urban form through structural rather than spectral information (Eddahby *et al.*, 2019). Sentinel-1 therefore adds a complementary perspective that may help distinguish between paved and unpaved road environments. Taken together, the three sensors offer complementary views of urban surfaces. Landsat-8 captures broader land-cover patterns, Sentinel-2 provides finer multispectral detail, and Sentinel-1 adds structural information about the built environment. Figure 3 shows the satellite imagery used in the study, with road networks overlaid in pink. Figure 3(a) presents Sentinel-1 SAR backscatter, Figure 3(b) shows Sentinel-2 optical imagery, and Figure 3(c) displays Landsat-8 optical imagery, each highlighting different surface characteristics and road patterns across the study area.

(a) (b) (c)

Figure 3. Multi-sensor comparison of surface characteristics and road network patterns in Greater Accra using Sentinel-1 SAR, Sentinel-2, and Landsat-8 imagery (2024).

2.3 Data Analysis

The data analysis was organised into a sequential workflow to prepare road network segments, extract satellite-derived features, train and validate classification models, detect road surface changes between 2018 and 2024, and identify spatial clusters of persistently unpaved roads.

All road geometries are converted to a projected coordinate system and segmented into uniform 100 m units to ensure spatial consistency. If a road has total length L (in meters), the number of segments (n) generated is defined as:

$$n = \left[\frac{L}{100}\right] \quad (1)$$

Where [] denotes the ceiling operator ensuring complete spatial coverage of each road. This segmentation guarantees that each analytical unit represents equal spatial length, thereby preventing longer roads from disproportionately influencing the learning process.

Following segmentation, satellite-derived features were extracted locally from exported raster imagery for each sensor–year combination. Three sensor configurations were analysed independently as shown in Figure 1: Landsat-8 (L8), Sentinel-2 (S2), and Sentinel-1 SAR (S1). For each year (2018 and 2024), the corresponding GeoTIFF imagery was read using a local raster processing workflow, features were sampled at five equally spaced points along each 100 m road segment, and the mean of the sampled pixel values was used to represent the segment after projection to a metric coordinate system (UTM Zone 30N). Sampling at multiple points along each segment provides a more representative measure of the road surface and reduces reliance on a single pixel.

For Landsat-8 and Sentinel-2, the extracted features included spectral bands (Blue, Green, Red, NIR, SWIR1, SWIR2) and derived indices computed directly from the raster stack. The Normalized Difference Vegetation Index (NDVI), Normalized Difference Built-up Index (NDBI), and a brightness index were further computed.

These indices enhance discrimination between vegetated, built-up, and compacted road surfaces by emphasizing spectral contrasts associated with asphalt, concrete, soil, and surrounding land cover. For Sentinel-1 SAR imagery, VV and VH polarization bands were extracted and converted to decibel scale where necessary using:

$$VVdB = 10\log10(VV) \quad (2)$$

$$VHdB = 10\log10(VH) \quad (3)$$

Additional polarization-derived features were computed as the difference

$$R_{pol} = VV_{dB}\text{-}VH_{dB} \quad (4)$$

and the ratio

$$R_{pol} = \frac{VV}{VH} \quad (5)$$

capturing surface roughness and structural variation relevant to road material characterization. Extracted pixel values were merged with segment identifiers, year, highway, and surface attributes to create a structured feature table per year and per sensor configuration, which was subsequently used for model training and prediction.

Road surface classification was conducted separately for 2018 and 2024 using Random Forest, XGBoost, and LightGBM models. These models were selected because they can handle nonlinear relationships and mixed feature types derived from optical and SAR imagery. For each road segment i, the model estimated the probability of belonging to the paved class based on the extracted feature vector X_i:

$$\hat{p}_i = P(yi = 1 \mid Xi) \quad (6)$$

where $y_i \in \{0,1\}$ represents the binary class label.

To ensure reliable performance estimates, a spatial validation strategy was applied to separate model training and validation data by location rather than random sampling. Road segments were grouped into geographic tiles of approximately 2 km × 2 km based on the projected coordinates of their centroids. For each cross-validation fold, one tile group served as the validation set while the remaining tiles formed the training set. Importantly, all preprocessing steps, including median imputation and quantile clipping (1st–99th percentile), were computed using the training folds only and then applied to the corresponding validation fold to prevent spatial leakage. Performance metrics were calculated from out-of-fold predictions aggregated across all folds, ensuring that each segment was

evaluated only by a model that had not been trained on that segment. No separate independent hold-out test was used in this study.

For each sensor configuration and year, model training used the feature table derived from the segmented road network. Only road segments with surface labels derived from OSM tags were used for supervised learning, while unlabelled segments were excluded from model fitting and used only during full prediction. The predictor variables consisted of the spectral bands, SAR backscatter values, and derived indices extracted from five equally spaced sample points along each 100 m segment and summarised using their mean values. Random Forest was implemented with 500 decision trees using balanced subsample weighting to address class imbalance. Additional parameters included max_features = 0.5, min_samples_split = 4, and min_samples_leaf = 1. XGBoost and LightGBM were implemented with 400 estimators and a learning rate of 0.05. For XGBoost, additional parameters included max_depth = 6, subsample = 0.8, and colsample_bytree = 0.8. For LightGBM, num_leaves = 31, subsample = 0.8, colsample_bytree = 0.8, and balanced class weighting were used. Each model outputs the probability that a road segment belongs to the paved class.

Out-of-fold (OOF) predicted probabilities were converted into binary class labels using a decision threshold T, which determines whether a road segment is classified as paved or unpaved. The predicted class label $\hat{y}_i$ for segment i is defined as:

$$\hat{y}_i = \begin{cases} 1, & if \quad \hat{p}_i > T \\ 0, & otherwise' \end{cases} \tag{7}$$

where $\hat{p}_i$ is the predicted probability of segment i belonging to the paved class and T is the classification threshold. The classification threshold T was determined using the out-of-fold predicted probabilities obtained from spatial cross-validation. A grid search was performed over candidate thresholds ranging from 0.05 to 0.95 in increments of 0.01. Thresholds that resulted in highly unbalanced predictions (i.e., nearly all segments classified into a single class) were excluded by requiring the proportion of predicted paved segments to fall between 5% and 95%. For each candidate threshold T, predicted probabilities were converted into binary class labels, and Balanced Accuracy was computed. The threshold that produced the highest Balanced Accuracy was selected as the optimal decision threshold. Balanced Accuracy is defined based on the components of the confusion matrix: true

positives (TP), true negatives (TN), false positives (FP), and false negatives (FN), providing a robust performance measure even under unequal class distributions. The MCC is a performance metric that evaluates the overall quality of a binary classification by measuring the agreement between predicted and actual classes while accounting for all outcomes of the confusion matrix. MCC is mathematically equivalent to a correlation coefficient between observed and predicted binary classifications and ranges from −1 to +1. In the context of this study, a value of +1 indicates perfect agreement between the predicted and observed road surface classes, meaning that all paved and unpaved road segments are correctly classified. A value of 0 indicates that the model performs no better than random assignment of paved and unpaved labels, while a value of −1 indicates complete disagreement, meaning that paved roads are consistently predicted as unpaved and vice versa.

Post-classification change detection was performed by spatially matching road segments across years using nearest-neighbour matching within a maximum distance of 15 m, allowing segments to be classified as upgraded, downgraded, or stable.

Let

$$\mathbf{y} = (y_{2018}, y_{2024}) \tag{8}$$

denote the predicted surface class vector, where $y_t \in \{0,1\}$, with 1 representing paved and 0 representing unpaved. The change status C is defined as:

$$C = \begin{cases} \text{Upgrade}, & \mathbf{y} = (0,1) \\ \text{Downgrade}, & \mathbf{y} = (1,0) \\ \text{Stable paved}, & \mathbf{y} = (1,1) \\ \text{Stable unpaved}, & \mathbf{y} = (0,0) \end{cases} \tag{9}$$

Roads that remained unpaved in both years were identified as stable unpaved and interpreted as persistent underdevelopment, while roads classified as unpaved in 2018 and paved in 2024 were identified as upgraded unpaved-to-paved segments, representing areas of surface improvement. To further examine the spatial structure of these patterns, both classes were analysed within a GIS environment. Their total lengths were first calculated across the full study area. In addition, both stable unpaved and upgraded unpaved-to-paved segments were clipped to the urban core boundary in order to quantify the length of each road class located within the urban core. This provided a basis for comparing persistent

underdevelopment and road upgrading in the most urbanised part of the region. For the stable unpaved class, the road segments were then converted into points at regular 50 m intervals to enable spatial density analysis while maintaining consistency with the original segmentation scale.

A Kernel Density Estimation (KDE) was applied to these points to generate a continuous surface representing the concentration of persistent unpaved roads. A bandwidth of 1000 m was selected to capture neighbourhood-scale patterns. The resulting density surface was then thresholded to extract areas of high concentration. The threshold was defined using the statistical distribution of KDE values, where areas exceeding the mean plus one standard deviation were classified as high-density clusters. For visualization purposes, the KDE surface was additionally displayed using equal-interval classes ranging from very low to very high. These high-density areas were converted into polygons representing candidate blind spot zones. To remove noise and ensure meaningful spatial interpretation, small polygons were excluded using a minimum area threshold derived from the distribution of polygon sizes. This step eliminates isolated fragments while retaining coherent spatial clusters. The remaining polygons were interpreted as blind spots, representing spatial clusters of persistent unpaved roads.

To support comparative analysis, the study area was represented using a regular grid of 2 km × 2 km cells. Grid cells intersecting blind spot polygons were excluded, resulting in a set of non-blindspot spatial units used for statistical comparison. To strengthen the spatial interpretation of these clusters, the identified blind spot polygons were further linked to administrative districts using a spatial join operation. This step assigns each blind spot to a named district, enabling the analysis to move beyond abstract spatial patterns to identifiable geographic locations within the Greater Accra Region. The resulting dataset allows for aggregation of blind spots by district, including area, and associated built-up intensity values, thereby supporting location-specific interpretation.

To provide a quantitative basis for interpreting spatial patterns, built-up intensity values derived from the Global Human Settlement Layer were incorporated into the analysis. The raster data were reprojected and aligned with the study area, and zonal statistics were used to extract mean built-up intensity values for both blind spot and non-blind spot areas. These values were exported for statistical analysis, enabling comparison of distributions, and supporting a structured evaluation of spatial differences between the two groups. Finally, spatial autocorrelation analysis was performed by defining a binary variable to distinguish blind spot and non-blinds pot areas (1 = blind spot, 0 = non-blind spot).

This variable was used to compute Moran's I, allowing assessment of the spatial clustering of persistent underdevelopment across the study area.

3. Results

This section presents the performance of the classification models, the spatial distribution of persistent road underdevelopment, and the statistical characteristics of identified blind spot areas in Accra.

3.1. Model Performance and Classification Accuracy

The findings reveal that model performance varied substantially by sensor type, algorithm, and year, as summarized in Table 1. These results were used to identify the most reliable sensor–algorithm configuration for detecting road surface condition across years. Landsat-8 models achieved strong and improved performance between years, with balanced accuracy ranging from approximately 0.72 to 0.73 in 2018 and increasing to 0.77 in 2024. Corresponding MCC values ranged from 0.44 to 0.46 in 2018 and improved to 0.52–0.53 in 2024, indicating enhanced class separability and model stability over time.

Sentinel-1–based models performed comparatively weakly in both years. In 2018, balanced accuracy ranged from approximately 0.57 to 0.58, with MCC values between 0.14 and 0.17. In 2024, performance remained low, with balanced accuracy between 0.54 and 0.57 and MCC values between 0.08 and 0.12, confirming limited discriminative power and persistent classification instability across all algorithms.

In contrast, Sentinel-2 consistently outperformed the other sensors. In 2018, balanced accuracy ranged from approximately 0.78 to 0.79, with MCC values between 0.57 and 0.58. Performance further improved in 2024, with balanced accuracy between 0.80 and 0.80 and MCC values between 0.58 and 0.58 across all algorithms.

Across algorithms, performance differences were small, with LightGBM and XGBoost consistently outperforming Random Forest. Under Sentinel-2, LightGBM achieved the highest performance (balanced accuracy ≈ 0.80; MCC ≈ 0.58), followed closely by XGBoost, while Random Forest performed slightly lower. A similar pattern is observed for Landsat-8 across both years.

Overall, sensor choice had a greater impact on performance than algorithm selection. The combination of Sentinel-2 and LightGBM produced the best results across both years and is therefore identified as the most reliable configuration for road surface classification in this study.

Table 1. Overall accuracy and Matthews Correlation Coefficient for road surface classification by sensor and algorithm in 2018 and 2024.

Sensor	Algorithm	2018 Accuracy	2018 MCC	2024 Accuracy	2024 MCC
Landsat-8	RF	0.723	0.448	0.767	0.520
	XGB	0.728	0.458	0.770	0.523
	LGBM	0.724	0.447	0.771	0.528
Sentinel-1	RF	0.569	0.142	0.543	0.083
	XGB	0.584	0.168	0.553	0.103
	LGBM	0.581	0.163	0.562	0.119
Sentinel-2	RF	0.787	0.575	0.796	0.577
	XGB	0.785	0.571	0.799	0.584
	LGBM	0.786	0.571	0.800	0.583

3.2. Classification Behaviour

To further interpret classification behaviour, the row-normalized confusion matrices for the S2_LGBM model are presented in Table 2. The results show that in 2018, the model correctly classified 77.92% of paved roads (TP) and 79.21% of unpaved roads (TN). Misclassification rates were relatively balanced, with 22.08% of paved roads incorrectly predicted as unpaved (FN) and 20.79% of unpaved roads incorrectly predicted as paved (FP).

A similar pattern is observed in 2024, where the model achieved 80.84% TP and 79.20% TN, with FN and FP rates of 19.16% and 20.80%, respectively. This consistency across years indicates that the S2_LGBM model maintains stable predictive behaviour over time, with no significant bias toward either class. The near-symmetric distribution of FP and FN further supports the robustness of the model, suggesting that classification errors are not systematically skewed toward overestimating either paved or unpaved road surfaces. Overall, the confusion matrix analysis reinforces the MCC findings, confirming that Sentinel-2–based models provide both high accuracy and balanced classification performance for road surface detection.

Table 2: Row-Normalized Confusion Matrices (%) for Road Surface Classification Using S2_LGBM Model (2018 and 2024).

Year		Predicted Paved	Predicted Unpaved
2018	Actual Paved	77.92% (TP)	22.08% (FN)
	Actual Unpaved	20.79% (FP)	79.21% (TN)
2024	Actual Paved	80.84% (TP)	19.16% (FN)
	Actual Unpaved	20.80% (FP)	79.20% (TN)

3.3. Spatial Distribution of Persistent Underdevelopment

Post-classification change detection from the 2018 to 2024 results are presented in Figure 4. Figure 4(a) shows road surface upgrades with 39.17% of its total within the urban core area out of its total length of 4068km in Greater Accra Region. In contrast, Figure 4(b) shows persistent unpaved roads with 18.97% of its total within the urban core area out of its total length of 11,031 km in Greater Accra Region. Furthermore, a total of 2092km length of persistent unpaved roads were found to be within the urban core area whereas a total of 1593km length of road surface upgrade were identified within the urban core.

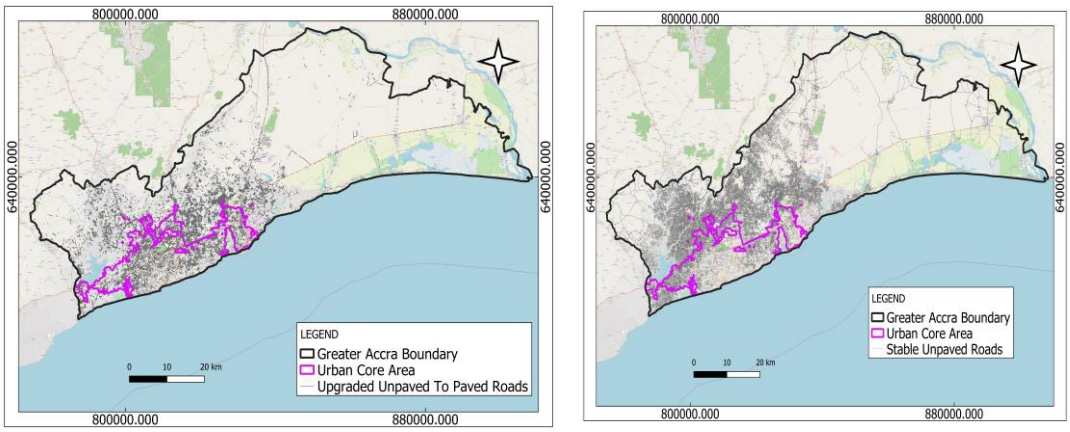

(a) (b)

Figure 4. Road surface change distribution in Greater Accra (2018–2024). (a) Road surface upgrades within core urban area. (b) Persistently unpaved roads within core urban area.

The spatial distribution of persistent unpaved roads is further examined in Figure 5, which presents both the density of these roads and the corresponding built-up context.

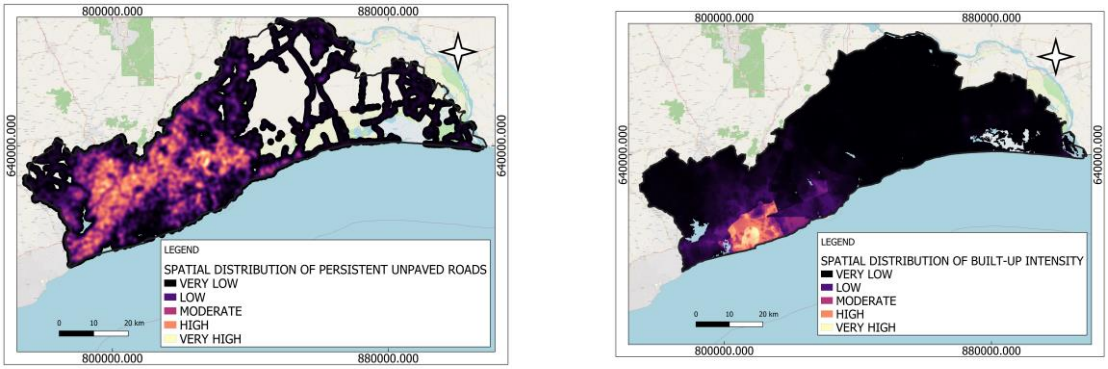

(a) (b)

Figure 5. Spatial distribution of persistent unpaved road density and built-up intensity in Greater Accra. (a) Kernel density of persistent unpaved roads. (b) Built-up intensity distribution

Figure 5(a) shows the kernel density surface of persistent unpaved roads, highlighting areas of very low to very high concentration across the study area. The results indicate that persistent unpaved roads are not uniformly distributed but instead form distinct spatial clusters. To provide additional spatial context, Figure 5(b) presents the distribution of built-up intensity across the study area, showing areas of very low to very high built-up values. This enables a direct comparison between the spatial

pattern of persistent unpaved road density and the distribution of built-up intensity. A comparison of the two maps shows that high to very high-density clusters of persistent unpaved roads occur across areas with varying levels of built-up intensity but are predominantly located outside areas characterized by high to very high built-up values. This indicates that persistent unpaved roads are more frequently associated with areas of lower to moderate built-up intensity, while areas with higher built-up values generally exhibit lower concentrations of persistent unpaved roads.

These high-density areas were delineated into discrete zones, referred to as blind spots, based on the threshold kernel density surface derived from Figure 5(a), as shown in Figure 6.

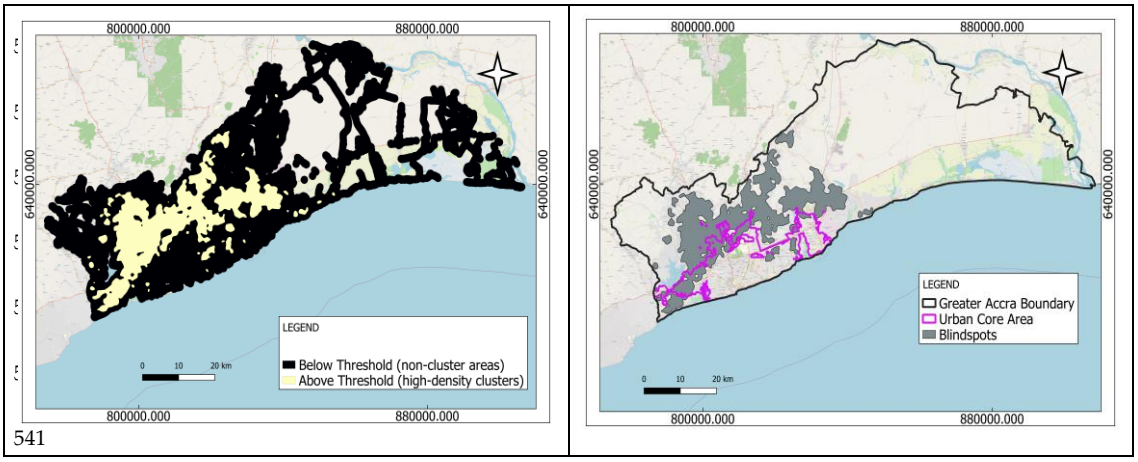

(a) (b)

Figure 6. Identified blind spot zones of persistent unpaved roads. (a) High-density clusters of persistent unpaved roads (0 = low-density areas, 1 = high-density areas). (b) Final blind spot zones after thresholding and filtering.

Figure 6(a) presents the classified high-density clusters of persistent unpaved roads, where values are defined as 0 (low-density areas or non-cluster areas) and 1 (high-density cluster areas). This binary classification highlight's locations where the concentration of persistent unpaved roads exceeds the defined threshold, distinguishing high-density clusters from the surrounding lower-density areas. Figure 6(b) shows the final blind spot zones after converting the high-density clusters into polygons and applying filtering procedures to remove smaller and less significant areas. A total of 14 blind spot areas were identified, covering approximately 566.891 km².

Spatially, these blind spots are distributed across multiple parts of the study area rather than being concentrated in a single location. Some occur as relatively large, continuous zones, while others appear

as smaller and more fragmented patches. Their spatial configuration reflects the clustering pattern of persistent unpaved roads within the broader road network.

3.4. District-Level Distribution of Blind Spots

To move beyond abstract spatial patterns, blind spot polygons were spatially linked to administrative districts across the study area. This approach ensured that blind spots intersecting multiple districts were appropriately partitioned and attributed to their respective administrative units. The results reveal that persistent underdevelopment is not evenly distributed across the region but is instead concentrated within a subset of districts, indicating a spatially uneven pattern of infrastructure provision. The district-level distribution of blind spots is summarized in Table 3, which presents the total blind spot area alongside the corresponding built-up intensity characteristics within each district.

Table 3. District-level distribution of blind spot areas and associated aggregate built-up area.

District	Blindspot area (km²)	Mean built-up intensity	Blindspot fragments
Kpone Katamanso Municipal	92.4910	11.2673	2
Ga West Municipal	76.2670	7.8535	4
Ga East Municipal	57.5530	24.8311	1
Ningo-Prampram	54.4310	3.8368	3
Ga North Municipal	49.5300	25.8332	1
Adentan Municipal	48.2320	9.7561	1
Ga Central Municipal	45.7570	25.1233	1
La Nkwantanang Madina Municipal	43.6360	16.5347	1
Ga South Municipal	43.4640	18.2846	4
Weija Gbawe Municipal	20.4950	40.4316	1
Shai-Osudoku	12.1140	2.7153	1
Tema West Municipal	9.8630	36.8303	3
Ledzokuku Municipal	5.5980	51.7391	1
Ashaiman Municipal	3.7070	45.7111	1

Krowor Municipal	1.6370	37.1559	1
Okaikoi North Municipal	1.5690	57.6845	1
Ablekuma North Municipal	0.1230	164.0629	1

A total of 17 out of 29 districts were identified as containing blind spot areas, demonstrating that persistent unpaved road clusters are geographically widespread but uneven in magnitude and intensity. The largest concentration of blind spot area is observed in Kpone Katamanso Municipal (92.491 km²), followed by Ga West Municipal (76.267 km²) and Ga East Municipal (57.553 km²). Other districts with substantial blind spot extents include Ningo-Prampram (54.431 km²), Ga North Municipal (49.530 km²), and Adentan Municipal (48.232 km²). These results indicate that persistent underdevelopment is not confined to isolated pockets but spans multiple districts.

In addition to spatial extent, built-up intensity within blind spot areas varies considerably across districts. Districts such as Ablekuma North Municipal (mean = 164.0629) and Okaikoi North Municipal (mean = 57.6845) exhibit exceptionally high built-up intensity values despite relatively small blind spot areas. Similarly, Ledzokuku Municipal (mean = 51.7391), Ashaiman Municipal (mean = 45.7111), and Weija Gbawe Municipal (mean = 40.4316) show elevated built-up intensity levels within blind spot zones. In contrast, districts such as Shai-Osudoku (mean = 2.7153) and Ningo-Prampram (mean = 3.8368) exhibit comparatively lower built-up intensity values.

The number of blind spot fragments also varies across districts, with Ga West Municipal and Ga South Municipal each containing multiple fragmented zones, while several districts contain only a single, spatially concentrated blind spot. This variation reflects differences in the internal spatial structure of underdevelopment, ranging from dispersed clusters to more localized concentrations.

3.5. Built-Up Characteristics and Statistical Differences

The differences in built-up characteristics between blind spot and non-blind spot areas are summarized in Table 4, which presents both aggregate spatial extent and the distribution of built-up intensity values.

Table 4. Built-up intensity statistics for blind spot and non-blind areas

(a) Aggregate area and central tendency

Group	Aggregate area (km²)	Mean built-up intensity	Median built-up intensity	Std built-up intensity
Blindspots	566.4670	26.8095	20.6829	31.5906
Non-blindspots	3132.2350	12.7755	2.1038	30.0062

(b) Built-up intensity distribution

Group	Count	Mean	Std	Min	25%	Median	75%	Max
Blindspots	28	26.8095	31.5906	2.4271	7.3852	20.6829	37.6164	164.0629
Non-blind-spots	1001	12.7755	30.0062	0.1435	0.6187	2.1038	7.0791	203.5665

Table 4(a) shows that non-blind spot areas occupy a substantially larger portion of the study area (3132.2350 km²) compared to blind spot areas (566.4670 km²). Despite this difference in spatial extent, blind spots exhibit higher built-up intensity. The mean built-up intensity for blind spots (26.8095) is more than twice that of non-blind areas (12.7755). This pattern is further reinforced by the median values, where blind spots (20.6829) substantially exceed non-blind areas (2.1038). These results indicate that blind spots are generally located in more built-up areas.

Further insights into the distribution of built-up intensity are provided in Table 4(b). Blind spot areas show consistently higher values across the distribution, with an interquartile range from 7.3852 to 37.6164, compared to 0.6187 to 7.0791 for non-blind areas. Notably, the lower quartile of blind spots (7.3852) exceeds the median of non-blind areas (2.1038), indicating a clear separation between the two groups.

The distribution in non-blind areas is highly skewed, as evidenced by the large difference between the mean (12.7755) and median (2.1038), suggesting that a small number of highly built-up locations

elevate the average while most areas remain weakly developed. In contrast, blind spot areas exhibit a more balanced distribution, with the mean (26.8095) and median (20.6829) being closer in magnitude.

Both groups display similar levels of variability, as indicated by comparable standard deviations (31.5906 for blind spots and 30.0062 for non-blind areas). However, this variability occurs around a higher baseline level in blind spot areas, reinforcing the observation that these areas are consistently more built-up.

3.6. Spatial Dependence

Statistical testing confirms that the observed differences in built-up intensity between blind spot and non-blind spot areas are not due to random variation. The Mann–Whitney U test shows a statistically significant difference between the two groups ($U = 22{,}718.0000$, $p = 0.0000$), indicating that the distributions of built-up intensity differ substantially. The Welch t-test also indicates a statistically significant difference in mean values ($t = 2.3216$, $p = 0.0276$), confirming that the difference between the groups is reflected not only in their distributions but also in their average levels.

The effect size, measured using Cliff's Delta ($\delta = 0.6211$), indicates a large difference between the two groups. This suggests that built-up intensity values in blind spot areas are generally higher than those in non-blind areas, consistent with the distributional patterns observed in Table 4.

In addition to these statistical differences, the spatial arrangement of blind spots exhibits significant clustering. The Moran's I value (0.0803) is higher than the expected value (−0.0010), indicating positive spatial autocorrelation. The associated Z-score (4.8600) and p-value (0.0010) confirm that this clustering pattern is statistically significant and unlikely to occur by chance.

Although the magnitude of Moran's I indicates moderate clustering strength, the results clearly show that blind spots are not randomly distributed across the study area but tend to occur in spatially grouped patterns.

Overall, these findings demonstrate that persistent road underdevelopment is both statistically distinct and spatially structured. When considered alongside the built-up intensity characteristics presented in Table 4, this indicates that blind spots are not only clustered in space but are also associated with specific urban conditions. This reinforces the conclusion that persistent underdevelopment is

spatially concentrated and systematically linked to patterns of urban development, rather than being randomly distributed across the region.

4. Discussion

The findings of this study provide strong empirical evidence that road infrastructure development in the Greater Accra Region is both spatially uneven and structurally persistent. Using multi-temporal classification and spatial analysis, the study shows that approximately 11,031 km of roads, representing 27.20% of the total road network, remained persistently unpaved between 2018 and 2024, indicating that a substantial portion of the road network has experienced no improvement over time. This persistence suggests that road underdevelopment is not merely a short-term condition but reflects relatively stable patterns over the study period.

A key finding is the clear urban–peripheral divide observed in the spatial distribution of road improvements. The results show that road surface upgrades are more concentrated in the urban core, with 1,593 km, representing 39.17% of all upgraded unpaved-to paved roads, located within the urban core. In contrast, persistently unpaved roads are less concentrated in the urban core, with 2,092 km, representing 18.97% of all persistently unpaved roads, located within this area. Although the urban core captures a larger share of road upgrading, the presence of over two thousand kilometres of persistently unpaved roads within the same area indicates that infrastructure improvement has been incomplete even in the most urbanised parts of the region. At the same time, the much larger share of persistent unpaved roads outside the urban core highlights the continued concentration of underdevelopment in peripheral areas. This pattern directly reflects uneven infrastructure provision across space and supports the argument that urban expansion in Greater Accra has not been matched by equivalent infrastructure development. Studies show urban growth in Greater Accra is spatially uneven and extends toward peripheral districts (Akubia and Bruns, 2019), likewise demonstrate that rapid expansion of built-up areas often outpaces effective infrastructure provision (Tossoukpe *et al.*, 2025). As a result, newly developed or expanding areas may remain underserved in terms of basic road infrastructure.

Beyond the general spatial pattern, the study further demonstrates that persistent underdevelopment is not randomly distributed but spatially clustered. Kernel density estimation identified distinct high-density clusters of persistently unpaved roads, which were delineated into 14 blind spot zones

covering approximately 566.9 km². The presence of these clusters is statistically confirmed by Moran's I (0.0803, p = 0.001), indicating significant spatial autocorrelation. This means that underdevelopment tends to concentrate in specific locations rather than being evenly spread across the region. Literature show that road infrastructure development in Accra can produce fragmented socio-spatial outcomes, supporting the interpretation that such clustering reflects underlying structural and planning dynamics rather than random variation (Adugbila, Martinez and Pfeffer, 2023)

At the district level, the results show that persistent underdevelopment is widespread but uneven in magnitude, affecting 17 out of 29 districts, with the largest concentrations found in districts such as Kpone Katamanso, Ga West, and Ga East. Importantly, these blind spots are not confined to a single geographic zone but appear across multiple parts of the metropolitan region, indicating that the problem is systemic rather than localized. The variation in both area and fragmentation of blind spots across districts further suggests differences in how underdevelopment manifests spatially, ranging from large continuous zones to smaller fragmented clusters.

One of the most important findings of this study is the relationship between persistent underdevelopment and built-up intensity. The results show that blind spot areas have significantly higher built-up intensity than non-blind areas, with mean values more than double (26.81 vs 12.78) and statistically significant differences confirmed by both Mann–Whitney and Welch tests. This indicates that persistent unpaved roads are not limited to sparsely developed or rural-like areas but are also found within relatively developed urban environments. This finding challenges the common assumption that infrastructure deficits are primarily associated with low-density or undeveloped areas. This interpretation is supported by studies using global settlement datasets such as the Global Human Settlement Layer. For instance, built-up density can increase independently of infrastructure provision (Melchiorri *et al.*, 2019), also demonstrating that GHSL data can reveal spatial mismatches between urban growth and service delivery (Melchiorri, 2022).

The implication of this result is important: urban development does not necessarily guarantee infrastructure provision. In some cases, areas with increasing built-up intensity still experience persistent road underdevelopment, suggesting a disconnect between urban growth and infrastructure investment. Infrastructure deficits in Ghana are strongly linked to insufficient investment and planning inefficiencies, which prevent infrastructure provision from keeping pace with rapid urbanisation. It also

reflects broader patterns where infrastructure provision is shaped by planning priorities and investment decisions rather than purely by demand or development intensity (Sarkodie Addo, Adu and Chinoperekweyi, 2023).

Furthermore, the coexistence of relatively high built-up intensity with persistent unpaved roads suggests that these areas may represent zones of incomplete or uneven integration into the urban system. In such contexts, residents may live in physically developed environments but still experience infrastructure deficits that affect mobility and accessibility. This aligns with research showing that infrastructure development can produce uneven socio-spatial outcomes, where some areas benefit more than others depending on planning and investment dynamics (Khanani *et al.*, 2021; Adugbila, Martinez and Pfeffer, 2023).

The findings also have implications for understanding mobility and accessibility. Since many of the persistently unpaved roads are located within neighbourhood and local road networks, their condition directly affects everyday mobility. Poor road conditions can limit connectivity, increase travel time, and restrict access to services and opportunities. Inadequate transport infrastructure constrains access to essential services and contributes to transport poverty (Popoola *et al.*, 2022), also unpaved roads in peri-urban areas significantly limit mobility and increase reliance on informal transport systems (Yakubu *et al.*, 2023). In this context, persistent road underdevelopment may act as a structural barrier to mobility, particularly for populations that rely on local road networks for daily movement.

The study's findings reinforce the interpretation of these clusters as policy blind spots, where infrastructure deficits persist despite surrounding urban development. The spatial persistence, clustering, and association with built-up areas indicate that these zones are not simply transitional or temporary gaps but represent areas that may have been repeatedly overlooked in infrastructure planning and investment processes. This is consistent with studies that show that infrastructure development in Accra can reinforce spatial inequalities and leave certain areas persistently underserved (Adugbila, Martinez and Pfeffer, 2023).

Finally, the results highlight the value of combining geospatial data and machine learning for infrastructure analysis in data-scarce environments. The ability to detect, quantify, and map persistent underdevelopment provides a more detailed understanding of where infrastructure gaps exist and how they are spatially organised. This addresses a key limitation in many African contexts, where reliable

data on road conditions is often lacking, making it difficult to support targeted infrastructure planning and intervention. (Zhou, Liu and Huang, 2024) similarly demonstrates that integrating OSM data with satellite imagery can effectively map road surface conditions at large scales, providing valuable support for infrastructure planning and decision-making.

5. Conclusion

In conclusion, this study demonstrates that road underdevelopment in the Greater Accra Region is persistent, spatially uneven, and strongly clustered. The results reveal clear spatial blind spots in road development and show that urban expansion has not been matched by equally distributed infrastructure improvement. These findings highlight the value of geospatial data and machine learning for identifying infrastructure gaps in rapidly urbanising, data-scarce environments. As a next step, we intend to explore convolutional neural network models for road-surface classification from satellite imagery and compare their performance with the present approach.

Supplementary Materials: The following supporting information can be downloaded from the project repository: https://doi.org/10.5281/zenodo.19928095

Author Contributions: Conceptualization, Desmond Kemeh and Yuri Ribakov; methodology, Desmond Kemeh; software, Desmond Kemeh; validation, Desmond Kemeh, Yuri Ribakov, Klein Israel and Achituv Cohen; formal analysis, Desmond Kemeh; investigation, Desmond Kemeh; resources, Desmond Kemeh, Yuri Ribakov, Klein Israel and Achituv Cohen; data curation, Desmond Kemeh; writing—original draft preparation, Desmond Kemeh; writing—review & editing, Yuri Ribakov, Klein Israel and Achituv Cohen; visualization, Desmond Kemeh; supervision, Yuri Ribakov and Achituv Cohen. All authors have read and agreed to the published version of the manuscript.

Funding: This research received no external funding

Data Availability Statement: The data and code supporting the findings of this study are publicly available in the following repository: https://doi.org/10.5281/zenodo.19928095. The repository

includes the full machine learning pipeline, statistical analysis scripts, QGIS project files, and processed datasets used to reproduce the results reported in this study.

Acknowledgments: The authors would like to thank Ariel University for providing the research environment and computational resources that supported this work. The authors acknowledge the use of QGIS for spatial analysis and mapping and Python (including GeoPandas, rasterio, scikit-learn, XGBoost, and LightGBM) for data processing, modelling, and statistical analysis.

Abbreviations: The following abbreviations are used in this manuscript:

OSM	OpenStreetMap
L8	Landsat-8
S2	Sentinel-2
S1	Sentinel-1
SAR	Synthetic Aperture Radar
NDVI	Normalized Difference Vegetation Index
NDBI	Normalized Difference Built-up Index
VV	Vertical transmit–Vertical receive polarization
VH	Vertical transmit–Horizontal receive polarization
RF	Random Forest
XGB	Extreme Gradient Boosting (XGBoost)
LGBM	Light Gradient Boosting Machine
KDE	Kernel Density Estimation
GHSL	Global Human Settlement Layer
UTM	Universal Transverse Mercator
OOF	Out-of-Fold
MCC	Matthews Correlation Coefficient
TPR	True Positive Rate
TNR	True Negative Rate

TP	True Positive
TN	True Negative
FP	False Positive
FN	False Negative

References

Acheampong, R.A., Asabere, S.B. and Asuah, A.Y. (2022) "Urban Form and Access to Public Transport in Accra, Ghana," in R.A. Acheampong et al. (eds.) *Transport and Mobility Futures in Urban Africa*. Cham: Springer International Publishing (The Urban Book Series), pp. 17–31. Available at: https://doi.org/10.1007/978-3-031-17327-1_3.

Addae, B. and Oppelt, N. (2019) "Land-Use/Land-Cover Change Analysis and Urban Growth Modelling in the Greater Accra Metropolitan Area (GAMA), Ghana," *Urban Science*, 3(1), p. 26. Available at: https://doi.org/10.3390/urbansci3010026.

Adugbila, E.J., Martinez, J.A. and Pfeffer, K. (2023a) "Road infrastructure expansion and socio-spatial fragmentation in the peri-urban zone in Accra, Ghana," *Cities*, 133, p. 104154. Available at: https://doi.org/10.1016/j.cities.2022.104154.

Adugbila, E.J., Martinez, J.A. and Pfeffer, K. (2023b) "Road infrastructure expansion and socio-spatial fragmentation in the peri-urban zone in Accra, Ghana," *Cities*, 133, p. 104154. Available at: https://doi.org/10.1016/j.cities.2022.104154.

Agyemang, E. *et al.* (2024) "Toward achieving smart cities in Africa: challenges to data use and the way forward," *Data & Policy*, 6, p. e13. Available at: https://doi.org/10.1017/dap.2024.11.

Akubia, J.E.K. and Bruns, A. (2019) "Unravelling the Frontiers of Urban Growth: Spatio-Temporal Dynamics of Land-Use Change and Urban Expansion in Greater Accra Metropolitan Area, Ghana," *Land*, 8(9), p. 131. Available at: https://doi.org/10.3390/land8090131.

Amedzro, K.K. *et al.* (2024) "Large-scale urban road corridors development and urban sprawl in the Greater Accra Metropolitan Area, Ghana," *International Development Planning Review*, 46(2), pp. 175–198. Available at: https://doi.org/10.3828/idpr.2024.2.

Antos, S.E., Lall, S.V. and Lozano-Gracia, N. (2016) *The Morphology of African Cities*. World Bank, Washington, DC. Available at: https://doi.org/10.1596/1813-9450-7911.

Brewer, E. *et al.* (2021) "Predicting road quality using high resolution satellite imagery: A transfer learning approach," *PLOS ONE*. Edited by T.R. Gadekallu, 16(7), p. e0253370. Available at: https://doi.org/10.1371/journal.pone.0253370.

Brussel, M. *et al.* (2019) "Access or Accessibility? A Critique of the Urban Transport SDG Indicator," *ISPRS International Journal of Geo-Information*, 8(2), p. 67. Available at: https://doi.org/10.3390/ijgi8020067.

Eddahby, L. *et al.* (2019) "SYNERGETIC USE OF SENTINEL-1 AND SENTINEL-2 DATA FOR EXTRACTION OF BUILT-UP AREA IN A ROCKY DESERT OASIS, EXAMPLE FOR DRAA TAFILALT, SOUTH-EAST OF MOROCCO," *The International Archives of the Photogrammetry, Remote Sensing and Spatial Information Sciences*, XLII-4/W12, pp. 65–68. Available at: https://doi.org/10.5194/isprs-archives-XLII-4-W12-65-2019.

El-bouayady, R. and Radoine, H. (2023) “Urbanization and Sustainable Urban Infrastructure Development in Africa,” *Environment and Ecology Research*, 11(2), pp. 385–391. Available at: https://doi.org/10.13189/eer.2023.110212.

Fobosi, S.C. and Malima, T. (2025) “Unveiling inequality: the sociological dynamics of road infrastructure development and social justice in rural Eastern Cape, South Africa,” *Frontiers in Sociology*, 9, p. 1481133. Available at: https://doi.org/10.3389/fsoc.2024.1481133.

Forget, Y. *et al.* (2021) “Mapping 20 Years of Urban Expansion in 45 Urban Areas of Sub-Saharan Africa,” *Remote Sensing*, 13(3), p. 525. Available at: https://doi.org/10.3390/rs13030525.

Forget, Y., Linard, C. and Gilbert, M. (2018) “Supervised Classification of Built-Up Areas in Sub-Saharan African Cities Using Landsat Imagery and OpenStreetMap,” *Remote Sensing*, 10(7), p. 1145. Available at: https://doi.org/10.3390/rs10071145.

Friesen, J., Georganos, S. and Haas, J. (2025) “Differences in walking access to healthcare facilities between formal and informal areas in 19 sub-Saharan African cities,” *Communications Medicine*, 5(1), p. 41. Available at: https://doi.org/10.1038/s43856-025-00746-5.

Gore, C.D. and Gopakumar, G. (2015) “Infrastructure and Metropolitan Reorganization: An Exploration of the Relationship in Africa and India,” *Journal of Urban Affairs*, 37(5), pp. 548–567. Available at: https://doi.org/10.1111/juaf.12180.

Hidayati, I., Tan, W. and Yamu, C. (2021) "Conceptualizing Mobility Inequality: Mobility and Accessibility for the Marginalized," *Journal of Planning Literature*, 36(4), pp. 492–507. Available at: https://doi.org/10.1177/08854122211012898.

Keith, M. and De Souza Santos, A.A. (eds.) (2021) "Introduction: Urban presence and uncertain futures in African cities," *African cities and collaborative futures*. Manchester University Press. Available at: https://doi.org/10.7765/9781526155351.00007.

Khalil, D. and Rubin, M. (2020) "Urban infrastructure and inequality," in N. Marrengane and S. Croese, *Re-framing the Urban Challenge in Africa*. 1st ed. London: Routledge, pp. 113–151. Available at: https://doi.org/10.4324/9781003008385-5.

Khanani, R.S. *et al.* (2021) "The Impact of Road Infrastructure Development Projects on Local Communities in Peri-Urban Areas: the Case of Kisumu, Kenya and Accra, Ghana," *International Journal of Community Well-Being*, 4(1), pp. 33–53. Available at: https://doi.org/10.1007/s42413-020-00077-4.

Korah, P.I., Matthews, T. and Tomerini, D. (2019) "Characterising spatial and temporal patterns of urban evolution in Sub-Saharan Africa: The case of Accra, Ghana," *Land Use Policy*, 87, p. 104049. Available at: https://doi.org/10.1016/j.landusepol.2019.104049.

Kyere-Gyeabour, E., Sivakumar, A. and Agyei-Mensah, S. (2024) "Transit and fairness: Exploring spatial equity in Accra's public transport system," *African Transport Studies*, 2, p. 100012. Available at: https://doi.org/10.1016/j.aftran.2024.100012.

Luz, G. *et al.* (2022) "Does better accessibility help to reduce social exclusion? Evidence from the City of São Paulo, Brazil." SocArXiv. Available at: https://doi.org/10.31235/osf.io/2p896.

Mahmoud, N. *et al.* (2022) "A Proposed Methodology for Detecting the Urban Footprint in Egypt," *IOP Conference Series: Earth and Environmental Science*, 992(1), p. 012008. Available at: https://doi.org/10.1088/1755-1315/992/1/012008.

Melchiorri, M. *et al.* (2019) "Principles and Applications of the Global Human Settlement Layer as Baseline for the Land Use Efficiency Indicator—SDG 11.3.1," *ISPRS International Journal of Geo-Information*, 8(2), p. 96. Available at: https://doi.org/10.3390/ijgi8020096.

Melchiorri, M. (2022) "The global human settlement layer sets a new standard for global urban data reporting with the urban centre database," *Frontiers in Environmental Science*, 10, p. 1003862. Available at: https://doi.org/10.3389/fenvs.2022.1003862.

Osman, A. *et al.* (2022) "Towards a concrete landscape: Assessing the efficiency of land consumption in the Greater Accra Region, Ghana," *PLOS ONE*. Edited by E. Ustaoglu, 17(6), p. e0269120. Available at: https://doi.org/10.1371/journal.pone.0269120.

Pesaresi, M. *et al.* (2016) "Assessment of the Added-Value of Sentinel-2 for Detecting Built-up Areas," *Remote Sensing*, 8(4), p. 299. Available at: https://doi.org/10.3390/rs8040299.

Phiri, D. *et al.* (2020) "Sentinel-2 Data for Land Cover/Use Mapping: A Review," *Remote Sensing*, 12(14), p. 2291. Available at: https://doi.org/10.3390/rs12142291.

Popoola, A. *et al.* (2022) "Transport Poverty: A Comparative Study between South Africa and Nigeria," *The Open Transportation Journal*, 16(1), p. e187444782207200. Available at: https://doi.org/10.2174/18744478-v16-e2207200.

Raji, T. *et al.* (2024) "Paved with Good Reflections: Road Quality Mapping with Multispectral Satellite Imagery," *Proceedings of the 11th ACM International Conference on Systems for Energy-Efficient Buildings, Cities, and Transportation*. *BuildSys '24: The 11th ACM International Conference on Systems for Energy-Efficient Buildings, Cities, and Transportation*, Hangzhou China: ACM, pp. 77–87. Available at: https://doi.org/10.1145/3671127.3698173.

Sarkodie Addo, F., Adu, D. and Chinoperekweyi, J. (2023) "Infrastructure Deficit and Social Challenges: The Ripple Effects on Sustainability in Ghana," *American Journal of Multidisciplinary Research and Innovation*, 2(5), pp. 13–21. Available at: https://doi.org/10.54536/ajmri.v2i5.1732.

Schwanen, T. *et al.* (2015) "Rethinking the links between social exclusion and transport disadvantage through the lens of social capital," *Transportation Research Part A: Policy and Practice*, 74, pp. 123–135. Available at: https://doi.org/10.1016/j.tra.2015.02.012.

Tossoukpe, A.Y. *et al.* (2025) "Dynamics of Changes in Spatial Patterns of Built-Up Areas in Two Metropolitan Areas of Grand Lomé and Greater Accra (West Africa)," *Urban Science*, 9(3), p. 84. Available at: https://doi.org/10.3390/urbansci9030084.

Wee, B.V., Wee, B.V. and Geurs, K. (2011) "Discussing Equity and Social Exclusion in Accessibility Evaluations," *European Journal of Transport and Infrastructure Research* [Preprint]. Available at: https://doi.org/10.18757/EJTIR.2011.11.4.2940.

Workman, R. *et al.* (2023) "Prediction of Unpaved Road Conditions Using High-Resolution Optical Satellite Imagery and Machine Learning," *Remote Sensing*, 15(16), p. 3985. Available at: https://doi.org/10.3390/rs15163985.

World Bank (2022) *Urban Mobility in African Cities*. Washington, DC. Available at: https://doi.org/10.1596/37082.

Yakubu, S. *et al.* (2023) "Movement on the Edge of Cities: Analysing Intra-urban Mobility in Peri-urban Communities in Southwest Nigeria," *Bulletin of Geography. Socio-economic Series*, (60), pp. 127–143. Available at: https://doi.org/10.12775/bgss-2023-0019.

Zhou, Q., Liu, Y. and Liu, Z. (2025) "Mapping National-Scale Road Surface Types Using Multisource Open Data and Deep Learning Model," *Transactions in GIS*, 29(1), p. e13305. Available at: https://doi.org/10.1111/tgis.13305.

Zhou, Q., Liu, Z. and Huang, Z. (2024) "Mapping Road Surface Type of Kenya Using OpenStreetMap and High-resolution Google Satellite Imagery," *Scientific Data*, 11(1), p. 331. Available at: https://doi.org/10.1038/s41597-024-03158-7.

Disclaimer/Publisher's Note: The statements, opinions and data contained in all publications are solely those of the individual author(s) and contributor(s) and not of MDPI and/or the editor(s). MDPI and/or the editor(s) disclaim responsibility for any injury to people or property resulting from any ideas, methods, instructions or products referred to in the content.